

# On the Adversarial Robustness of Camera-based 3D Object Detection

Shaoyuan Xie<sup>1</sup> Zichao Li<sup>2</sup> Zeyu Wang<sup>2</sup> Cihang Xie<sup>2</sup>

<sup>1</sup>Huazhong University of Science and Technology <sup>2</sup>University of California, Santa Cruz

## Abstract

In recent years, camera-based 3D object detection has gained widespread attention for its ability to achieve high performance with low computational cost. However, the robustness of these methods to adversarial attacks has not been thoroughly examined. In this study, we conduct the first comprehensive investigation of the robustness of leading camera-based 3D object detection methods under various adversarial conditions. Our experiments reveal five interesting findings: (a) the use of accurate depth estimation effectively improves robustness; (b) depth-estimation-free approaches do not show superior robustness; (c) bird’s-eye-view-based representations exhibit greater robustness against localization attacks; (d) incorporating multi-frame benign inputs can effectively mitigate adversarial attacks; and (e) addressing long-tail problems can enhance robustness. We hope our work can provide guidance for the design of future camera-based object detection modules with improved adversarial robustness.

## 1. Introduction

Deep neural network-based 3D object detectors, such as those presented in [13, 15, 18, 21, 37–40, 43, 44], have demonstrated promising performance on various challenging real-world benchmarks, including the KITTI [9], Waymo [32], and nuScenes [3] datasets. These popular approaches utilize either point clouds [15, 37, 43, 44] or images [13, 17, 18, 21, 38–40] as inputs for detection tasks. In comparison to LIDAR-based methods, camera-based approaches have garnered significant attention due to their low deployment cost, high computational efficiency, and dense semantic information. Additionally, camera-based detection exhibits inherent advantages in detecting long-range objects and identifying vision-based traffic signs.

Monocular 3D object detection, as described in [38, 39], expands the scope of 2D object detection to 3D scenarios using carefully designed custom adaptations. However, accurately estimating depth from a single image is a difficult problem, and as a result, inaccurate depth estimation is a major impediment to the performance of monocular 3D

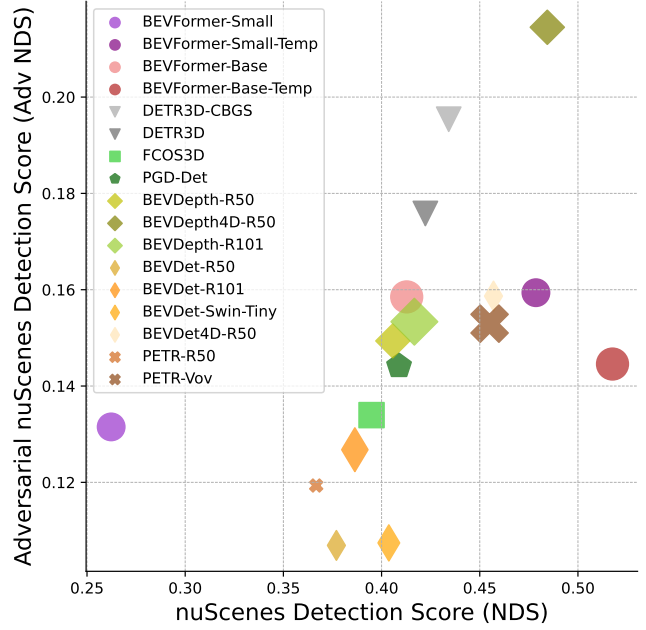


Figure 1. Adversarial NDS vs. clean NDS. The adversarial NDS is evaluated by averaging all attack types under all attack severities. Robustness is evaluated using nuScenes-mini [3] subset, while clean NDS is evaluated using full nuScenes [3] validation set. The scatter sizes are proportional to model parameter sizes.

object detection [38]. In contrast, using a bird’s eye view (BEV) for 3D detection offers several advantages. First, it allows for joint learning from multi-view images. Second, the bird’s eye perspective provides a physics-interpretable method for fusing information from different sensors and time stamps [24]. Third, the output space of a BEV-based approach can be easily applied to downstream tasks such as prediction and planning. Consequently, BEV-based detection frameworks have demonstrated significant improvements [12, 13, 17, 18].

Despite the significant progress made by recent camera-based 3D object detection methods, their robustness to adversarial attacks is not yet well understood. This motivates us to investigate the robustness of these approaches under malicious attacks. Previous research has demonstrated that 3D perception systems can be easily compro-

misled by adversarial examples [4, 30, 35], posing potential safety threats. However, these works primarily focus on causing a few targeted models to crash under specific conditions. To the best of our knowledge, the robustness of camera-based 3D object detection has not yet been systematically studied.

To address this gap in knowledge, we conduct the first comprehensive study on the adversarial robustness of camera-based 3D object detectors. Specifically, we generate pixel-based, patch-based, and black-box adversarial examples under real-world conditions to evaluate the robustness of these models. Our focus is on two main attack goals: confusing classification predictions and confusing localization predictions. Regarding pixel attacks, we apply the widely-used projected gradient descent (PGD) algorithm [25]. To differentiate this attack algorithm from the 3D detection method known as Probabilistic and Geometric Depth [38], we refer to the former as PGD-Adv and the latter as PGD-Det in the rest of the paper. Regarding patch attacks, we superimpose a patch onto the input image, where the patch pattern is optimized via gradient descent [2]. The patches are placed at the center of targets, and their sizes are dynamically adjusted according to the size of the object and the distance from the sensors, making our approach more physically realistic. We also explore the use of universal patches, which can transfer across scenes, scales, and models. Based on these settings, we conduct extensive experiments and make the following interesting findings:

- Accurate depth estimation is of paramount importance for models that rely on depth information for transforming the perspective view to a bird’s eye view. The incorporation of explicit depth supervision during training, as well as prior knowledge of depth constraints, can lead to improved performance and stronger robustness.
- While depth-estimation-free methods have achieved state-of-the-art performance with clean inputs [18, 21, 40], we find they generally do not yield stronger robustness compared to depth-estimation-based ones.
- BEV-based models may not exhibit stronger robustness under classification attacks. However, they tend to be more robust towards localization attacks.
- Adversarial effects can be mitigated through the use of temporal information, meaning that models utilizing multi-frame benign inputs are less likely to fail under single-frame attacks. However, it is important to note that errors can accumulate under continuous adversarial input over multiple frames.
- Resampling training strategies such as Class Balanced Group Sampling (CBGS) [45], which aim to address long-tail problems, may enhance model robustness.



Figure 2. Examples of patch-based attacks. Top: fixed 25x25 pixel patch size. Bottom: dynamic patch size with a scale of 0.3 proportional to the 2D bounding box of the target.

## 2. Related Work

**Camera-based 3D object detection.** Existing camera-based 3D object detection methods can be broadly categorized into two groups: monocular-based approaches [38, 39] and bird’s eye view (BEV)-based approaches [12, 13, 17, 18, 21, 40]. Monocular-based approaches, such as FCOS3D and PGD-Det [38, 39], extend FCOS [34] to the 3D domain through specific adaptations. BEV-based detectors transform the perspective view to BEV to perform perception tasks. Inspired by LSS [27], BEVDet [13] uses an additional depth estimation branch for the perspective-to-BEV transformation. BEVDet4D [12] further improves performance by leveraging temporal information. BEVDepth [17] improves depth estimation accuracy through explicit depth supervision from point clouds. Another line of work performs the perspective-to-BEV transformation without an explicit depth estimation branch. Following DETR [5], DETR3D represents 3D objects as object queries and performs cross-attention using a Transformer decoder [36]. PETR [21, 22] further improves performance by proposing 3D position-aware representations. BEVFormer [18] introduces spatial and temporal cross-attention to extract BEV features from multi-view and multi-timestamp images.

**Adversarial attacks on classification.** Modern neural networks have been shown to be susceptible to adversarial attacks [10, 26, 33], where the addition of a carefully crafted perturbation to the input can cause the network to make an

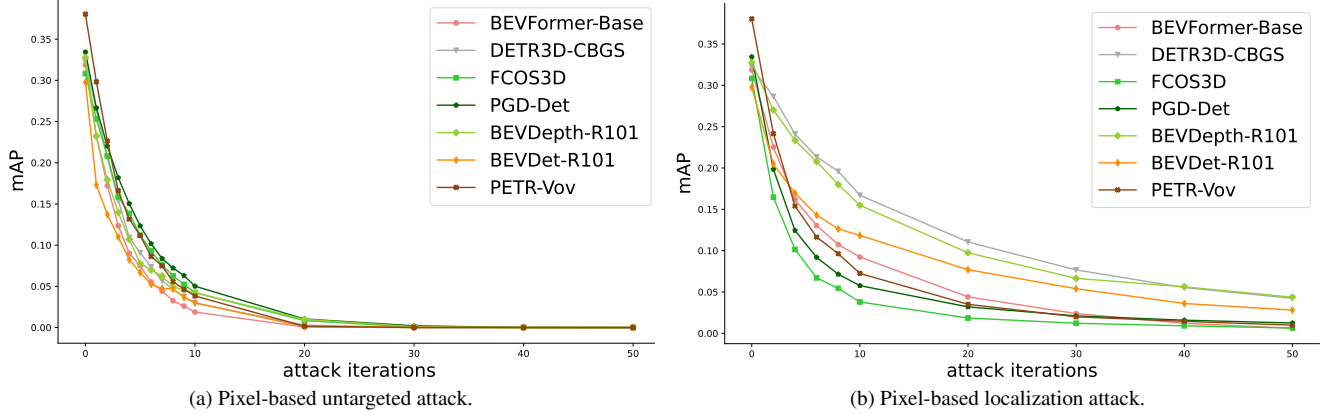


Figure 3. mAP value vs. attack iterations. The plotted BEVDet [13], BEVDepth [17], and PETR-Vov [21] are trained with CBGS [45].

incorrect prediction. In [10], a simple and efficient method for generating adversarial examples using one-step gradient descent is proposed. Madry *et al.* [25] propose more powerful attacks (*i.e.*, PGD-Adv) by taking multiple steps along the gradients and projecting the perturbation back onto an  $L_p$  norm ball. Moosavi-Dezfooli *et al.* [26] demonstrate the existence of universal adversarial perturbations. Brown *et al.* [2] generate physical adversarial patches. Liu *et al.* [20] study the transferability of both non-targeted and targeted adversarial examples and introduce an ensemble-based approach for generating more transferable adversarial examples. Wu *et al.* [41] address adversarial robustness in the context of long-tailed distribution recognition tasks. In addition to developing more powerful attacks, some works have focused on understanding the robustness of different neural architecture designs to attacks. [1, 31] conduct extensive comparisons between CNNs and Transformers and gain insights into their adversarial robustness.

**Adversarial attacks on object detection.** Adversarial attacks for object detection can target both localization and classification. For 2D object detection, Xie *et al.* [42] generate adversarial examples with strong transferability by considering all targets densely. Liu *et al.* [19] propose black-box patch attacks that can compromise the performance of popular frameworks such as Faster R-CNN [29] and YOLO [28]. Given the crucial importance of safety in autonomous driving, it is vital to study the adversarial robustness of 3D object detection. Tu *et al.* [35] craft adversarial mesh placed on top of a vehicle to bypass a LiDAR detector. Rossolini *et al.* [30] study digital, simulated, and physical patches to mislead real-time semantic segmentation models. Cao *et al.* [4] reveals the possibility of crashing Multi-Sensor Fusion (MSF) based models by attacking all fusion sources simultaneously. However, to the best of our knowledge, the robustness of camera-based 3D object detection models to adversarial attacks has not yet been systematically studied, and this is the main focus of this work.

### 3. Camera-based 3D Object Detection

In this section, we provide an overview of the current leading approaches in camera-based 3D object detection, which can be broadly classified into three categories: monocular-based detectors, BEV detectors with depth estimation, and BEV detectors without depth estimation.

#### 3.1. Monocular Approach

This line of research aims to directly predict 3D targets from an image input. We select FCOS3D [39] and PGD-Det [38] as representative works to study their adversarial robustness. FCOS3D [39] extends FCOS [34] to the 3D domain by transforming 3D targets to the image domain. PGD-Det [38] further improves the performance of FCOS3D [39] by incorporating uncertainty modeling and constructing a depth propagation graph that leverages the interdependence between instances.

#### 3.2. BEV Detector with Depth Estimation

This line of work first predicts a per-pixel depth map, maps image features to corresponding 3D locations, and subsequently predicts 3D targets in the BEV perspective. Building on the success of the BEV paradigm in the BEV semantic segmentation task, BEVDet [13] develops the first high-performance BEV detector based on the Lift-Splat-Shoot (LSS) view transformer [27]. Subsequently, BEVDet4D [12] introduces multi-frame fusion to improve the effectiveness of temporal cue learning. BEVDepth [17] proposes to use point cloud projection to the image plane for direct supervision of depth estimation. Note that this approach can also incorporate temporal fusion, which we refer to as BEVDepth4D.

We hereby aim to evaluate the robustness of these BEV models, ranging from the most basic detector (*i.e.*, BEVDet) to spatial (Depth) and temporal (4D) extensions, against adversarial attacks.

### 3.3. BEV Detector without Depth Estimation

In this set of works, the trainable sparse object queries are utilized to aggregate image features without the need for depth estimation. Representative examples of this type of approach include DETR3D [40], which connects 2D feature extraction and 3D bounding box prediction through backward geometric projection; PETR [21, 22], which enhances 2D features with 3D position-aware representations; and BEVFormer [18], which refines BEV queries using spatial and temporal cross-attention mechanisms.

## 4. Generating Adversarial Examples

In this section, we introduce our algorithms to generate adversarial examples. We consider three different settings: pixel-based white-box attacks, patch-based white-box attacks, and universal patch black-box attacks.

### 4.1. Pixel-based Attack

Given an input image  $I \in \mathbb{R}^{C \times H \times W}$ , 3D object detectors output the perception results including class, 3D bounding boxes, and other attributes, *i.e.*,  $f(I) = cls, loc, vel, \dots \in \mathbb{R}^n$ . These prediction results are compared to ground truth bounding boxes  $T = t_1, t_2, t_3, \dots, t_N$ , where a match is made if their 2D center distances on the ground plane are smaller than a certain threshold, as in [3]. We hereby investigate the robustness of the models against adversarial attacks targeting the classification, localization, velocity, and orientation predictions. To generate adversarial examples, our goal is to make the prediction results go wrong. Specifically, for classification attacks, we aim to fool the model predicts a wrong class, *i.e.*,  $f_{cls}(I + r, t_n) \neq l_n$ . To achieve this, we use an untargeted attack and maximize the cross-entropy loss:

$$\mathcal{L}_{untargeted} = -\frac{1}{N} \sum_{i=1}^N \sum_{j=1}^C f_j(I + r, t_i) \log p_{ij}, \quad (1)$$

where  $C$  denotes the number of classes,  $r$  denotes the adversarial perturbation and  $f_j$  denotes the confidence score on  $j$ -th class. The adversarial perturbation  $r$  is optimized iteratively using PGD-Adv [25] as:

$$r_{i+1} = \text{Proj}_\epsilon(r_i + \alpha \text{sgn}(\nabla_{I+r_i} \mathcal{L})). \quad (2)$$

To ensure a fair comparison, the confidence scores are normalized between  $[0, 1]$  using the sigmoid function to avoid sensitivity to logits range [41]. Maximizing  $\mathcal{L}_{untargeted}$  can be achieved by making every target incorrectly predicted. For targeted attacks, we specify an adversarial label  $l'_n \neq l_n$  for each target. The adversarial objective [6] can then be written as:

$$\mathcal{L}_{targeted} = \frac{1}{N} \sum_{i=1}^N [f_{l'_n}(I + r, t_i) - f_{l_n}(I + r, t_i)]. \quad (3)$$

To confuse localization or other attributes, we find it is sufficient to adopt a simple  $\mathcal{L}_1$  loss as the objective function:

$$\begin{aligned} \mathcal{L}_{localization} = & \frac{1}{N} \sum_{i=1}^N \|f_{loc}(I + r, t_i) - loc_i\|_1 \\ & + \|f_{orie}(I + r, t_i) - orie_i\|_1 \\ & + \|f_{vel}(I + r, t_i) - vel_i\|_1. \end{aligned} \quad (4)$$

### 4.2. Patch-based Attack

Attackers are able to generate physical adversarial patches attached to the center of objects for misleading detectors in real-world settings. Given that target objects can vary in size and distance from the sensors, we dynamically adjust the patch size based on the 2D bounding box of the target. Specifically, for a target with a 3D bounding box that has 8 corners and 1 center point, denoted as  $c_o, c_1, \dots, c_8$ , where  $c_i \in \mathbb{R}^3$ , we project these 3D points to 2D points on the image plane,  $c'_o, c'_1, \dots, c'_8$ , using the extrinsic and intrinsic parameters of the camera. The patch size is proportional to the exterior rectangle formed by these 2D points and is placed at the center point  $c'_o$ , as illustrated in Fig. 2. The final assignment and adversarial loss function used in this patch-based attack are the same as those described in Sec. 4.1.

### 4.3. Black-box Attack

We are also interested in studying the existence of universal adversarial patches for 3D object detection. We first define and randomly initialize a fixed-size patch, which is then applied to the center of the object as described in Sec. 4.2. The patch is resized dynamically based on the size of the object using bilinear interpolation. Following [6], we optimize the pattern of the patch using the Adam optimizer [14]. During testing, we apply the generated patch to unseen images, and further to other network architectures. The generated adversarial patch is considered transferable if it can always confuse models under different scales, input images, and model architectures.

## 5. Experiments

### 5.1. Experimental Setup

**Dataset and metric.** We conduct experiments on the popular autonomous driving nuScenes dataset [3], which contains data captured using six cameras, one LiDAR, and five radars. The dataset is composed of 1000 scenarios, which are split into 700, 150, and 150 scenes for training, validation, and testing, respectively. Additionally, we also evaluate our results on a subset of the dataset, nuScenes-mini [3], which contains 484 images. To evaluate the performance of our approach, we use the Mean Average Precision (mAP) and nuScenes Detection Score (NDS) metrics.

Models	Image Size	param	clean NDS	Adv NDS	clean mAP	Adv mAP
BEVFormer-Small [18]	1280 × 720	59.6M	0.2623	0.1315	0.1324	0.0567
BEVFormer-Base [18]	1600 × 900	69.1M	0.4128	0.1585	0.3461	0.0833
DETR3D [40]	1600 × 900	53.8M	0.4223	0.1758	0.3469	0.1081
DETR3D <sup>†</sup> [40]	1600 × 900	53.8M	0.4342	<u>0.1953</u>	0.3494	<u>0.1126</u>
PETR-R50 [21]	1408 × 512	38.1M	0.3667	0.1193	0.3174	0.0641
PETR-VovNet <sup>†</sup> [21]	1600 × 640	83.1M	0.4550	0.1529	<u>0.4035</u>	0.0838
BEVDepth-R50 <sup>†</sup> [17]	704 × 257	53.1M	0.4057	0.1493	0.3327	0.0923
BEVDepth-R101 <sup>†</sup> § [17]	704 × 257	72.1M	0.4167	0.1533	0.3376	0.1007
BEVDet-R50 <sup>†</sup> [13]	704 × 257	48.2M	0.3770	0.1069	0.2987	0.0634
BEVDet-R101 <sup>†</sup> § [13]	704 × 257	67.2M	0.3864	0.1267	0.3021	0.0754
BEVDet-Swin-Tiny <sup>†</sup> [13]	704 × 257	55.9M	0.4037	0.1074	0.3080	0.0635
FCOS3D [39]	1600 × 900	55.1M	0.3949	0.1339	0.3214	0.0714
PGD-Det [38]	1600 × 900	56.2M	0.4089	0.1441	0.3360	0.0843
BEVFormer-Small# [18]	1280 × 720	59.6M	0.4786	0.1593	0.3699	0.1007
BEVFormer-Base# [18]	1600 × 900	69.1M	<b>0.5176</b>	0.1445	<b>0.4167</b>	0.0846
BEVDepth4D-R50 <sup>†</sup> # [17]	704 × 257	53.4M	<u>0.4844</u>	<b>0.2144</b>	0.3609	<b>0.1211</b>
BEVDet4D-R50 <sup>†</sup> # [12]	704 × 257	48.2M	0.4570	0.1586	0.3215	0.0770

Table 1. Overall adversarial NDS: clean results are evaluated on nuScenes [3] validation set, and adversarial results are evaluated on the mini subset. The adversarial NDS is averaged for all the attack types and severities. <sup>†</sup>trained with CBGS [45], §are re-trained models with minimal modification since there is no publicly available checkpoint, # use temporal information.

**Experiment settings.** We evaluate our models using publicly available models and in cases where the checkpoints are not publicly available, we retrain them with minimal modifications. To assess the performance of our models, we evaluate both the clean performance and adversarial robustness. Specifically, clean performance is evaluated on the entire validation set, while adversarial robustness is evaluated on the small nuScenes-mini dataset. Our implementation is based on the open-sourced MMDetection3D [7].

## 5.2. Pixel-based Attacks

We first evaluate pixel-based adversarial attacks using perturbations under the  $L_\infty$  norm. We set the maximum value to  $\epsilon = 5$ , and the step size is fixed at  $\alpha = 0.1$ . We first add Gaussian noise to randomly perturb the inputs, and then gradually increase the number of attack iterations from 1 to 50 for both untargeted attacks and localization attacks. If no prediction results are assigned to the ground truth, the iteration stops accordingly.

Note that the nuScenes dataset captures six images per scene, but the overlaps between them are relatively small. As a result, we only evaluate attacks on individual cameras. The results are illustrated in Fig. 3, and the average adversarial mAP and NDS are presented in Tab. 2. Furthermore, it is important to note that the BEVFormer model [18] maintains historical BEV features for temporal cross-attention, meaning that attacks on previous frames can also affect current predictions, simulating real-world scenarios where attackers continuously attack multiple frames.

Models	Adv NDS	Adv mAP
BEVFormer-Small [18]	0.1170	0.0284
BEVFormer-Base [18]	0.1562	0.0621
DETR3D [40]	0.1700	0.0796
DETR3D <sup>†</sup> [40]	<u>0.1921</u>	0.0766
PETR-R50 [21]	0.1256	0.0559
PETR-VovNet <sup>†</sup> [21]	0.1708	0.0883
BEVDepth-R50 <sup>†</sup> [17]	0.1339	0.0646
BEVDepth-R101 <sup>†</sup> § [17]	0.1436	0.0726
BEVDet-R50 <sup>†</sup> [13]	0.0806	0.0377
BEVDet-R101 <sup>†</sup> § [13]	0.1121	0.0559
BEVDet-Swin-Tiny <sup>†</sup> [13]	0.0856	0.0406
FCOS3D [39]	0.1536	0.0861
PGD-Det [38]	0.1696	0.0947
BEVFormer-Small# [18]	0.1727	<u>0.0964</u>
BEVFormer-Base# [18]	0.1328	0.0555
BEVDepth4D-R50 <sup>†</sup> # [17]	<b>0.2143</b>	<b>0.0969</b>
BEVDet4D-R50 <sup>†</sup> # [12]	0.1394	0.0473

Table 2. Pixel-based untargeted attacks, the adversarial NDS and mAP are averaged under 14 sample points (*i.e.*, different attack iterations) on the attack curve.

For localization attacks, we modify the adversarial objective to focus on the  $L_1$  loss of the localization, orientation, and velocity predictions, while keeping all other settings unchanged. The results are shown in Tab. 3. We find that the performance of the models behaves differently

Models	Adv NDS	Adv mAP
BEVFormer-Small [18]	0.1310	0.0836
BEVFormer-Base [18]	0.1390	0.0892
DETR3D [40]	0.1709	0.1454
DETR3D <sup>†</sup> [40]	<u>0.1873</u>	<b>0.1543</b>
PETR-R50 [21]	0.1170	0.0786
PETR-VovNet <sup>†</sup> [21]	0.1321	0.0844
BEVDepth-R50 <sup>†</sup> # [17]	0.1626	0.1301
BEVDepth-R101 <sup>†</sup> # [17]	0.1691	0.1455
BEVDet-R50 <sup>†</sup> [13]	0.1244	0.0932
BEVDet-R101 <sup>†</sup> # [13]	0.1406	0.1063
BEVDet-Swin-Tiny <sup>†</sup> [13]	0.1058	0.0746
FCOS3D [39]	0.1103	0.0524
PGD-Det [38]	0.1105	0.0694
BEVFormer-Small# [18]	0.1221	0.0949
BEVFormer-Base# [18]	0.1312	0.1017
BEVDepth4D-R50 <sup>†</sup> # [17]	<b>0.1914</b>	<u>0.1488</u>
BEVDet4D-R50 <sup>†</sup> # [12]	0.1499	0.1031

Table 3. The average result of pixel-based localization attacks, where attackers aim to confuse detectors’ localization, orientation, and velocity predictions.

under localization attacks as compared to untargeted attacks, as shown in Fig. 3. Furthermore, we observe that the BEV-based models consistently outperform monocular approaches, which rely on implicitly learning depth information from single camera inputs.

### 5.3. Patch-based Attacks

We next evaluate model robustness against patch-based attacks. To initialize the patch pattern, we use a Gaussian Distribution with a mean and variance equal to the dataset. The step size is set to  $\alpha = 5$ , and the number of attack iterations is fixed at 50. We gradually increase the patch scale from 0.1 to 0.4. The results, including the average adversarial NDS and mAP, can be found in tables Tab. 4 and Tab. 5. In general, we find that the adversarial effect of superimposing patch patterns on target objects is milder compared to pixel-based PGD-Adv attacks. Furthermore, we observe that attacks that aim to confuse classification are more harmful than perturbing localization, a trend similar to pixel-based PGD-Adv attacks. However, BEVDepth [17] with temporal modeling exhibits strong robustness against all types of attacks.

### 5.4. Transfer Black-box Attacks

Lastly, we study the robustness of our models against black-box attacks. Specifically, we optimize the patch using the training set of the nuScenes mini subset [3], which has 1938 images. We set the learning rate to 10, the patch size to  $100 \times 100$ , and the scale to  $s = 0.3$ . We use targeted

Models	Adv NDS	Adv mAP
BEVFormer-Small [18]	0.1428	0.0425
BEVFormer-Base [18]	0.1775	0.0713
DETR3D [40]	0.1797	0.0664
DETR3D <sup>†</sup> [40]	<u>0.2021</u>	0.0753
PETR-R50 [21]	0.0887	0.0338
PETR-VovNet <sup>†</sup> [21]	0.1352	0.0511
BEVDepth-R50 <sup>†</sup> [17]	0.1339	0.0603
BEVDepth-R101 <sup>†</sup> # [17]	0.1301	0.0577
BEVDet-R50 <sup>†</sup> [13]	0.1102	0.0397
BEVDet-R101 <sup>†</sup> # [13]	0.1176	0.0401
BEVDet-Swin-Tiny <sup>†</sup> [13]	0.1365	0.0632
FCOS3D [39]	0.1225	0.0543
PGD-Det [38]	0.1126	0.0612
BEVFormer-Small# [18]	0.1746	<u>0.0907</u>
BEVFormer-Base# [18]	0.1689	0.0766
BEVDepth4D-R50 <sup>†</sup> # [17]	<b>0.2388</b>	<b>0.0960</b>
BEVDet4D-R50 <sup>†</sup> # [12]	0.1887	0.0633

Table 4. The average results of untargeted patch untargeted attacks. Note the adversarial NDS, and mAP are averaged under 4 sample points (*i.e.*, different patch scales) on the attack curve.

Models	Adv NDS	Adv mAP
BEVFormer-Small [18]	0.1720	0.1096
BEVFormer-Base [18]	0.1910	0.1560
DETR3D [40]	0.2030	0.1663
DETR3D <sup>†</sup> [40]	<u>0.2183</u>	<b>0.1824</b>
PETR-R50 [21]	0.1330	0.0911
PETR-VovNet <sup>†</sup> [21]	0.1548	0.0989
BEVDepth-R50 <sup>†</sup> [17]	0.1891	0.1366
BEVDepth-R101 <sup>†</sup> # [17]	0.1751	0.1414
BEVDet-R50 <sup>†</sup> [13]	0.1562	0.1107
BEVDet-R101 <sup>†</sup> # [13]	0.1558	0.1094
BEVDet-Swin-Tiny <sup>†</sup> [13]	0.1580	0.1191
FCOS3D [39]	0.1296	0.0799
PGD-Det [38]	0.1621	0.1049
BEVFormer-Small# [18]	0.1810	0.1388
BEVFormer-Base# [18]	0.1910	0.1559
BEVDepth4D-R50 <sup>†</sup> # [17]	<b>0.2425</b>	<u>0.1687</u>
BEVDet4D-R50 <sup>†</sup> # [12]	0.2157	0.1358

Table 5. The average result of patch localization attacks, where attackers aim to confuse detectors’ localization, orientation, and velocity predictions.

attacks as the adversarial objective, where we aim to misclassify all categories as “Car” and attack “Car” to “Pedestrian”. In the inference stage, we apply the trained patch to unseen scenes and different models with dynamic sizes. To account for the occlusion caused by the patch itself, we

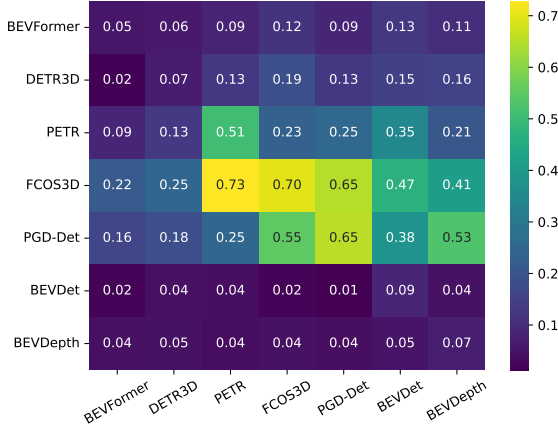


Figure 4. Universal patch targeted attacks. The X-axis represents the target model, and Y-axis represents the source model. The transferability is measured as the relative performance (i.e., mAP) drop compared to a random patch pattern of the same size.

use a random pattern patch as a baseline and calculate the relative performance drop. The results are shown in Fig. 4. Interestingly, universal patches generated by FCOS3D [39] and PGD-Det [38] transfer well across models. For example, transferring attacks from FCOS3D [39] to PETR [21] can result in a relative performance drop of more than 70%. In contrast, BEVDet [13] and BEVDepth [17] are less vulnerable to this type of attack and generate adversarial examples with limited transferability.

## 6. Discussion

### 6.1. BEV-based vs. Non-BEV-based Models

To study whether BEV detectors still outperform monocular detectors under adversarial attacks, we selected four models for comparison: BEVDet [13], BEVDepth [17], FCOS3D [39], and PGD-Det [38]. These models are chosen as their clean performance is similar and they all use ResNet101 [11] as the backbone. The results are shown in Fig. 5. We find that BEV-based methods do not exhibit superior robustness against untargeted attacks. Moreover, all the models are vulnerable to untargeted classification attacks, with nearly all the mAP values dropping to 0 under 20 attack iterations. Note that the difference among the methods under untargeted attacks is relatively small when compared to localization attacks, as shown in Fig. 3.

On the other hand, BEV-based models demonstrate superior performance under localization attacks. Under pixel-based perturbations, the adversarial NDS of BEVDepth [17] outperforms PGD-Det [38] by  $\sim 53\%$ . This trend can also be observed in Fig. 3b, where all BEV-based approaches outperform monocular approaches. Additionally, when applying patch-based attacks, BEV-based models continue to demonstrate an advantage over monocular models, although the advantage is slightly smaller (see Tab. 5).

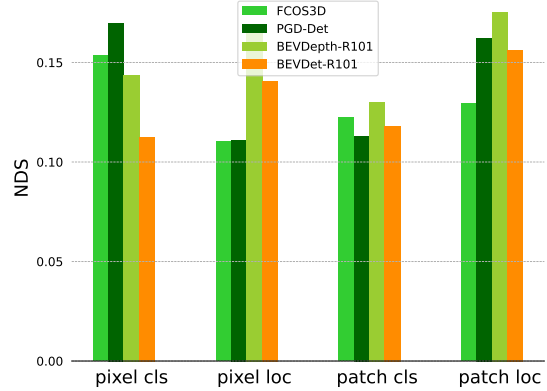


Figure 5. BEV-based model vs. Non-BEV-based model under 4 types of attacks. All the backbones are ResNet101 [11] with DCN [8] and without temporal information.

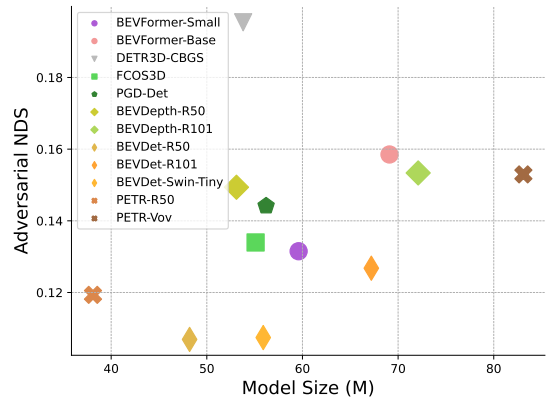


Figure 6. Model size vs. Adversarial NDS. On top of DETR3D [40], BEVformer [18] introduces spatial and temporal attention for extracting BEV features, but the extra encoder does not contribute to adversarial robustness. Modules that intend to improve depth estimation consistently help robustness. For the same architecture, enlarging the model size consistently helps robustness.

### 6.2. Network Architecture

We investigate the impact of different backbone architectures, including ResNet [11], VoVNet [16], and Swin-Transformer [23], on the robustness of models. We first compare Swin-Tiny and ResNet50, as their backbone sizes are similar (23.6M vs. 27.5M). Although they perform slightly differently under various attacks, the overall robustness of ResNet50 and Swin-Tiny is similar (i.e., 0.1069 vs. 0.1074). On the other hand, increasing the backbone size consistently leads to improved robustness. This trend is more prominent for models with weaker robustness (i.e., from BEVDet-R50 [13] to BEVDet-R101 [13] and from PETR-R50 [21] to PETR-Vov [21]). Surprisingly, we find that the additional BEV encoders in BEVFormer [18] do not contribute to adversarial robustness, despite improving clean performance, as shown in Fig. 6. This suggests that modules that improve performance do not necessarily increase robustness.



Figure 7. Depth estimation results. From top to bottom: original FRONT camera images, BEVDepth [17] depth prediction results, BEVDet [13] depth prediction results. Accurate depth estimation provides the model with strong robustness.

### 6.3. Depth Estimation

In our analysis, we found that models with more accurate depth estimation exhibit stronger robustness against adversarial attacks. This can be observed in Tab. 1, where the PGD-Det [38] improves upon FCOS3D [39] by using better depth estimation and shows consistent robustness improvement under all types of attacks. Additionally, the BEVDet [13] and BEVDepth [17] models, which differ only in their depth estimation module, showed that the accurate depth estimation in BEVDepth [17] provided a 39.6% increase in adversarial NDS (0.1493 vs. 0.1069). Furthermore, we found that depth-estimation-free approaches [18, 21, 40] do not show clear advantages over detectors with explicit depth estimation in terms of adversarial robustness. More interestingly, we note that depth-estimation-based approaches demonstrate competitive or even superior performance compared to depth-estimation-free methods under localization attacks (see Fig. 3b).

### 6.4. CBGS Training

Open object detection challenges often have long-tail properties, where the numbers of some categories (*e.g.*, Car, Pedestrian) greatly exceed others (*e.g.*, Motorcycle). We find that strategies designed to address long-tail problems, such as Class Balanced Group Sampling (CBGS) training [45], can also improve robustness. Our results show that DETR3D trained with CBGS [45] improves adversar-

ial NDS by  $\sim 11\%$  (0.1953 vs. 0.1758). This conclusion differs from the prior work [41], which found that resampling training strategies had little effect on robustness. Nonetheless, it is important to note that our study considers different settings and objectives, and our methods differ from those used in [41].

### 6.5. Temporal Information

Incorporation of temporal information from previous frames has been shown to consistently improve detection performance [12, 17, 18]. To investigate the impact of temporal information on adversarial robustness, we propose two attack scenarios. For BEVFormer [18], since the model updates its history BEV queries on-the-fly, we attack each individual input frame. This means that all sequential inputs used for temporal information modeling are adversarial examples, leading to an accumulation of errors within the model through stored temporal information. Our experiments show that the BEVFormer-Base model [18] performs worse when using temporal information compared to its single frame input counterpart (*i.e.*, 0.1585 vs. 0.1445). In the second scenario, we attack the current timestamp input while maintaining clean history information. We test BEVDepth4D [17] and BEVDet4D [12] under this setting, which combines features from the current frame and a recent historical frame in their predictions. As shown in Tab. 1, we find that clean temporal information significantly reduces the adversarial effect in this scenario, with 0.1493 vs. 0.2144 for BEVDepth [17], and 0.1069 vs. 0.1586 for BEVDet [12, 17].

### 6.6. Black-box Transferability

Surprisingly, the universal patches generated by some victim models, such as FCOS3D [39], are even more harmful than the patches generated by the target model itself, such as BEVDepth [17]. These patches transferred effectively to unseen images and different methods, resulting in a relative performance drop of at least 20%. It is worth noting that the patch, even when resized using bilinear interpolation, remained adversarial. Our findings indicate that monocular models generally produce stronger black-box adversarial examples with high transferability, even to BEV-based models. This is a significant potential threat, as any risk is intolerable for autonomous driving systems.

## 7. Conclusions

We hereby conducted a thorough examination of the adversarial robustness of camera-based 3D object detection models. Our findings reveal model robustness does not necessarily align with its clean performance. Additionally, we identified several strategies that can enhance robustness. We hope that our research provides valuable insights for the development of more robust models in the future.

## Acknowledgement

This work is supported by a gift from Open Philanthropy and UCSC Office of Research Seed Funding for Early Stage Initiatives.

## References

- [1] Yutong Bai, Jieru Mei, Alan L Yuille, and Cihang Xie. Are transformers more robust than cnns? *Advances in Neural Information Processing Systems*, 34:26831–26843, 2021. [1](#), [2](#), [3](#), [5](#), [6](#), [7](#), [8](#), [11](#)
- [2] Tom B Brown, Dandelion Mané, Aurko Roy, Martín Abadi, and Justin Gilmer. Adversarial patch. *arXiv preprint arXiv:1712.09665*, 2017. [2](#), [3](#)
- [3] Holger Caesar, Varun Bankiti, Alex H Lang, Sourabh Vora, Venice Erin Liong, Qiang Xu, Anush Krishnan, Yu Pan, Giancarlo Baldan, and Oscar Beijbom. nuscenes: A multi-modal dataset for autonomous driving. In *Proceedings of the IEEE/CVF conference on computer vision and pattern recognition*, pages 11621–11631, 2020. [1](#), [4](#), [5](#), [6](#), [11](#)
- [4] Yulong Cao, Ningfei Wang, Chaowei Xiao, Dawei Yang, Jin Fang, Ruigang Yang, Qi Alfred Chen, Mingyan Liu, and Bo Li. Invisible for both camera and lidar: Security of multi-sensor fusion based perception in autonomous driving under physical-world attacks. In *2021 IEEE Symposium on Security and Privacy (SP)*, pages 176–194. IEEE, 2021. [2](#), [3](#)
- [5] Nicolas Carion, Francisco Massa, Gabriel Synnaeve, Nicolas Usunier, Alexander Kirillov, and Sergey Zagoruyko. End-to-end object detection with transformers. In *European conference on computer vision*, pages 213–229. Springer, 2020. [2](#)
- [6] Nicholas Carlini and David Wagner. Towards evaluating the robustness of neural networks. In *2017 IEEE Symposium on Security and Privacy (SP)*, pages 39–57. Ieee, 2017. [4](#)
- [7] MMDetection3D Contributors. MMDetection3D: OpenMMLab next-generation platform for general 3D object detection. <https://github.com/open-mmlab/mmdetection3d>, 2020. [5](#)
- [8] Jifeng Dai, Haozhi Qi, Yuwen Xiong, Yi Li, Guodong Zhang, Han Hu, and Yichen Wei. Deformable convolutional networks. In *Proceedings of the IEEE international conference on computer vision*, pages 764–773, 2017. [7](#)
- [9] Andreas Geiger, Philip Lenz, and Raquel Urtasun. Are we ready for autonomous driving? the kitti vision benchmark suite. In *2012 IEEE conference on computer vision and pattern recognition*, pages 3354–3361. IEEE, 2012. [1](#)
- [10] Ian J Goodfellow, Jonathon Shlens, and Christian Szegedy. Explaining and harnessing adversarial examples. *arXiv preprint arXiv:1412.6572*, 2014. [2](#), [3](#)
- [11] Kaiming He, Xiangyu Zhang, Shaoqing Ren, and Jian Sun. Deep residual learning for image recognition. In *Proceedings of the IEEE conference on computer vision and pattern recognition*, pages 770–778, 2016. [7](#)
- [12] Junjie Huang and Guan Huang. Bevdet4d: Exploit temporal cues in multi-camera 3d object detection. *arXiv preprint arXiv:2203.17054*, 2022. [1](#), [2](#), [3](#), [5](#), [6](#), [8](#)
- [13] Junjie Huang, Guan Huang, Zheng Zhu, and Dalong Du. Bevdet: High-performance multi-camera 3d object detection in bird-eye-view. *arXiv preprint arXiv:2112.11790*, 2021. [1](#), [2](#), [3](#), [5](#), [6](#), [7](#), [8](#), [11](#)
- [14] Diederik P Kingma and Jimmy Ba. Adam: A method for stochastic optimization. *arXiv preprint arXiv:1412.6980*, 2014. [4](#)
- [15] Alex H Lang, Sourabh Vora, Holger Caesar, Lubing Zhou, Jiong Yang, and Oscar Beijbom. Pointpillars: Fast encoders for object detection from point clouds. In *Proceedings of the IEEE/CVF conference on computer vision and pattern recognition*, pages 12697–12705, 2019. [1](#)
- [16] Youngwan Lee, Joong-won Hwang, Sangrok Lee, Yuseok Bae, and Jongyoul Park. An energy and gpu-computation efficient backbone network for real-time object detection. In *Proceedings of the IEEE/CVF conference on computer vision and pattern recognition workshops*, pages 0–0, 2019. [7](#)
- [17] Yinhao Li, Zheng Ge, Guanyi Yu, Jinrong Yang, Zengran Wang, Yukang Shi, Jianjian Sun, and Zeming Li. Bevdepth: Acquisition of reliable depth for multi-view 3d object detection. *arXiv preprint arXiv:2206.10092*, 2022. [1](#), [2](#), [3](#), [5](#), [6](#), [7](#), [8](#), [11](#)
- [18] Zhiqi Li, Wenhao Wang, Hongyang Li, Enze Xie, Chonghao Sima, Tong Lu, Qiao Yu, and Jifeng Dai. Bevformer: Learning bird’s-eye-view representation from multi-camera images via spatiotemporal transformers. *arXiv preprint arXiv:2203.17270*, 2022. [1](#), [2](#), [4](#), [5](#), [6](#), [7](#), [8](#), [11](#)
- [19] Xin Liu, Huanrui Yang, Ziwei Liu, Linghao Song, Hai Li, and Yiran Chen. Dpatch: An adversarial patch attack on object detectors. *arXiv preprint arXiv:1806.02299*, 2018. [3](#)
- [20] Yanpei Liu, Xinyun Chen, Chang Liu, and Dawn Song. Delving into transferable adversarial examples and black-box attacks. *arXiv preprint arXiv:1611.02770*, 2016. [3](#)
- [21] Yingfei Liu, Tiancai Wang, Xiangyu Zhang, and Jian Sun. Petr: Position embedding transformation for multi-view 3d object detection. *arXiv preprint arXiv:2203.05625*, 2022. [1](#), [2](#), [3](#), [4](#), [5](#), [6](#), [7](#), [8](#), [11](#)
- [22] Yingfei Liu, Junjie Yan, Fan Jia, Shuailin Li, Qi Gao, Tiancai Wang, Xiangyu Zhang, and Jian Sun. PetrV2: A unified framework for 3d perception from multi-camera images. *arXiv preprint arXiv:2206.01256*, 2022. [2](#), [4](#)
- [23] Ze Liu, Yutong Lin, Yue Cao, Han Hu, Yixuan Wei, Zheng Zhang, Stephen Lin, and Baining Guo. Swin transformer: Hierarchical vision transformer using shifted windows. In *Proceedings of the IEEE/CVF International Conference on Computer Vision*, pages 10012–10022, 2021. [7](#)
- [24] Yuexin Ma, Tai Wang, Xuyang Bai, Huitong Yang, Yuenan Hou, Yaming Wang, Yu Qiao, Ruigang Yang, Dinesh Manocha, and Xinge Zhu. Vision-centric bev perception: A survey. *arXiv preprint arXiv:2208.02797*, 2022. [1](#)
- [25] Aleksander Madry, Aleksandar Makelov, Ludwig Schmidt, Dimitris Tsipras, and Adrian Vladu. Towards deep learning models resistant to adversarial attacks. *arXiv preprint arXiv:1706.06083*, 2017. [2](#), [3](#), [4](#)
- [26] Seyed-Mohsen Moosavi-Dezfooli, Alhussein Fawzi, Omar Fawzi, and Pascal Frossard. Universal adversarial perturbations. In *Proceedings of the IEEE conference on computer vision and pattern recognition*, pages 1765–1773, 2017. [2](#), [3](#)

- [27] Jonah Philion and Sanja Fidler. Lift, splat, shoot: Encoding images from arbitrary camera rigs by implicitly unprojecting to 3d. In *European Conference on Computer Vision*, pages 194–210. Springer, 2020. 2, 3
- [28] Joseph Redmon, Santosh Divvala, Ross Girshick, and Ali Farhadi. You only look once: Unified, real-time object detection. In *Proceedings of the IEEE conference on computer vision and pattern recognition*, pages 779–788, 2016. 3
- [29] Shaoqing Ren, Kaiming He, Ross Girshick, and Jian Sun. Faster r-cnn: Towards real-time object detection with region proposal networks. *Advances in neural information processing systems*, 28, 2015. 3
- [30] Giulio Rossolini, Federico Nesti, Gianluca D’Amico, Saasha Nair, Alessandro Biondi, and Giorgio Buttazzo. On the real-world adversarial robustness of real-time semantic segmentation models for autonomous driving. *arXiv preprint arXiv:2201.01850*, 2022. 2, 3
- [31] Rulin Shao, Zhouxing Shi, Jinfeng Yi, Pin-Yu Chen, and Cho-Jui Hsieh. On the adversarial robustness of vision transformers. *arXiv preprint arXiv:2103.15670*, 2021. 3
- [32] Pei Sun, Henrik Kretschmar, Xerxes Dotiwalla, Aurelien Chouard, Vijaysai Patnaik, Paul Tsui, James Guo, Yin Zhou, Yuning Chai, Benjamin Caine, et al. Scalability in perception for autonomous driving: Waymo open dataset. In *Proceedings of the IEEE/CVF conference on computer vision and pattern recognition*, pages 2446–2454, 2020. 1
- [33] Christian Szegedy, Wojciech Zaremba, Ilya Sutskever, Joan Bruna, Dumitru Erhan, Ian Goodfellow, and Rob Fergus. Intriguing properties of neural networks. *arXiv preprint arXiv:1312.6199*, 2013. 2
- [34] Zhi Tian, Chunhua Shen, Hao Chen, and Tong He. Fcos: Fully convolutional one-stage object detection. In *Proceedings of the IEEE/CVF international conference on computer vision*, pages 9627–9636, 2019. 2, 3
- [35] James Tu, Mengye Ren, Sivabalan Manivasagam, Ming Liang, Bin Yang, Richard Du, Frank Cheng, and Raquel Urtasun. Physically realizable adversarial examples for lidar object detection. In *Proceedings of the IEEE/CVF Conference on Computer Vision and Pattern Recognition*, pages 13716–13725, 2020. 2, 3
- [36] Ashish Vaswani, Noam Shazeer, Niki Parmar, Jakob Uszkoreit, Llion Jones, Aidan N Gomez, Łukasz Kaiser, and Illia Polosukhin. Attention is all you need. *Advances in neural information processing systems*, 30, 2017. 2
- [37] Sourabh Vora, Alex H Lang, Bassam Helou, and Oscar Beijbom. Pointpainting: Sequential fusion for 3d object detection. In *Proceedings of the IEEE/CVF conference on computer vision and pattern recognition*, pages 4604–4612, 2020. 1
- [38] Tai Wang, ZHU Xinge, Jiangmiao Pang, and Dahua Lin. Probabilistic and geometric depth: Detecting objects in perspective. In *Conference on Robot Learning*, pages 1475–1485. PMLR, 2022. 1, 2, 3, 5, 6, 7, 8
- [39] Tai Wang, Xinge Zhu, Jiangmiao Pang, and Dahua Lin. Fcos3d: Fully convolutional one-stage monocular 3d object detection. In *Proceedings of the IEEE/CVF International Conference on Computer Vision*, pages 913–922, 2021. 1, 2, 3, 5, 6, 7, 8
- [40] Yue Wang, Vitor Campagnolo Guizilini, Tianyuan Zhang, Yilun Wang, Hang Zhao, and Justin Solomon. Detr3d: 3d object detection from multi-view images via 3d-to-2d queries. In *Conference on Robot Learning*, pages 180–191. PMLR, 2022. 1, 2, 4, 5, 6, 7, 8, 11
- [41] Tong Wu, Ziwei Liu, Qingqiu Huang, Yu Wang, and Dahua Lin. Adversarial robustness under long-tailed distribution. In *Proceedings of the IEEE/CVF conference on computer vision and pattern recognition*, pages 8659–8668, 2021. 3, 4, 8
- [42] Cihang Xie, Jianyu Wang, Zhishuai Zhang, Yuyin Zhou, Lingxi Xie, and Alan Yuille. Adversarial examples for semantic segmentation and object detection. In *Proceedings of the IEEE international conference on computer vision*, pages 1369–1378, 2017. 3
- [43] Yan Yan, Yuxing Mao, and Bo Li. Second: Sparsely embedded convolutional detection. *Sensors*, 18(10):3337, 2018. 1
- [44] Yin Zhou and Oncel Tuzel. Voxelnet: End-to-end learning for point cloud based 3d object detection. In *Proceedings of the IEEE conference on computer vision and pattern recognition*, pages 4490–4499, 2018. 1
- [45] Benjin Zhu, Zhengkai Jiang, Xiangxin Zhou, Zeming Li, and Gang Yu. Class-balanced grouping and sampling for point cloud 3d object detection. *arXiv preprint arXiv:1908.09492*, 2019. 2, 3, 5, 8

## A. Full Adversarial Attacks Result

In this part, we list the full experiment results. We present the mAP and NDS metrics of all the models under 4 types of attacks (*i.e.*, the attack iterations or the patch scale). For each attack, we use multiple attack severities to minimize randomness. We set the random seed to 0 for all experiments. The curves are plotted in Fig. 9, Fig. 10, Fig. 11, and Fig. 12.

## B. Dynamical Patch vs. Fixed Patch

We compare the results of the dynamical patch and fixed-sized patch. In our paper, we choose to use dynamical size patches because it is more physically reasonable. Real-world patch size changes according to distance from sensors. Attackers only need a smaller patch for pedestrians to fool the detectors while might need a larger one for larger objects (*i.e.*, Car and Bus). As a result, it is not reasonable nor fair to apply a fixed patch size to every object. To explain the difference, we calculate the detection results of each class, the comparison can be seen in Fig. 8. The results are evaluated using BEVFormer-base [18] with temporal information on nuScenes [3] mini validation set. We calculate the relative AP drop compared to clean input.

## C. Black-Box Transfer Attacks

Here we provide the full results of universal patch-based black box transfer attacks as shown in Tab. 6 and Tab. 7. We conduct universal patch attacks using BEVFormer-base [18] without temporal information, DETR3D [40], PETR-R50 [21], BEVDepth-R101 [17], and BEVDet-R50 [13]. Among the above models, DETR3D [40], BEVDet [13], and BEVDepth [17] are trained with CBGS strategy. Considering the occlusion induced by patches, we randomly initialize the patch with the same size to serve as the baseline.

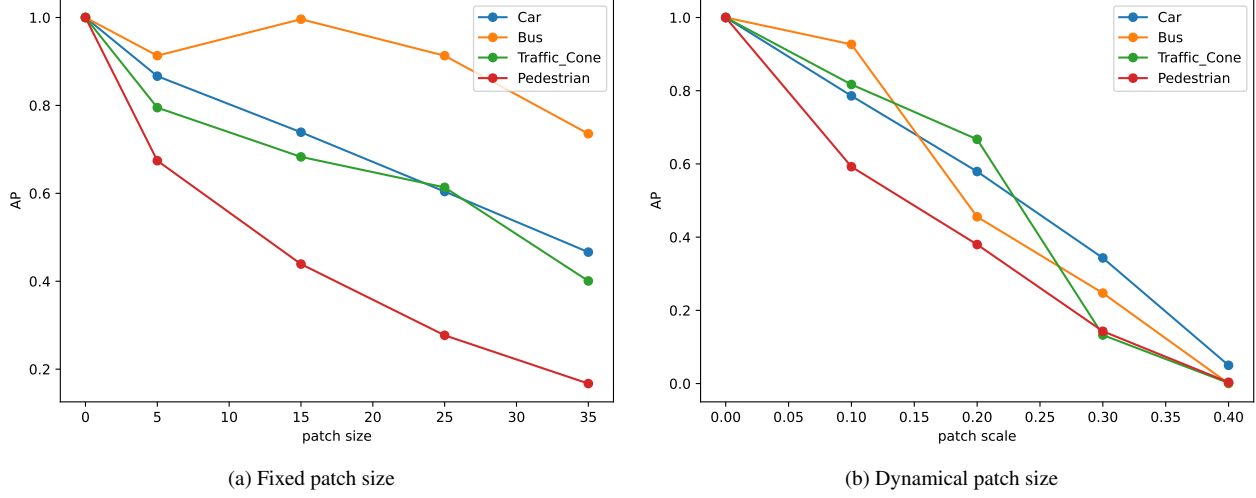


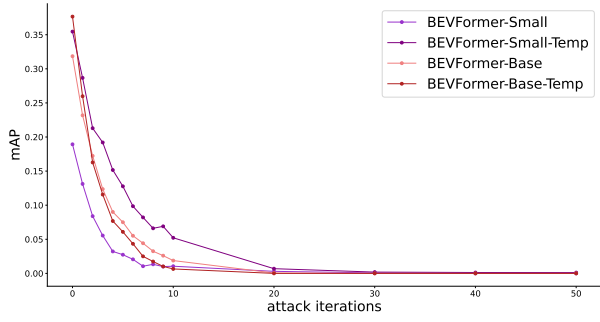
Figure 8. Patch size ablation: We calculate relative performance drop ( *i.e.*, AP) of several classes. When applying fixed-size patches, the performance drop of small objects is much more drastic than large objects. When applying dynamical patch size, each class’s performance drop is more balanced.

Adversarial Source	BEVFormer	DETR3D	PETR	FCOS3D	PGD-Det	BEVDet	BEVDepth
Random Noise	0.2816	0.3014	0.2515	0.2379	0.2546	0.1924	0.2380
BEVFormer	0.2663	0.2827	0.2301	0.2098	0.2316	0.1676	0.2132
DETR3D	0.2767	0.2799	0.2195	0.1936	0.2221	0.1634	0.2017
PETR	0.2561	0.2613	0.1236	0.1825	0.1904	0.1256	0.1895
FCOS3D	0.2205	0.2266	0.0683	0.0724	0.0893	0.1018	0.1410
PGD-Det	0.2357	0.2463	0.1805	0.1069	0.0879	0.1186	0.1128
BEVDet	0.2760	0.2807	0.2416	0.2334	0.2513	0.1758	0.2283
BEVDepth	0.2693	0.2874	0.2422	0.2275	0.2445	0.1829	0.2213

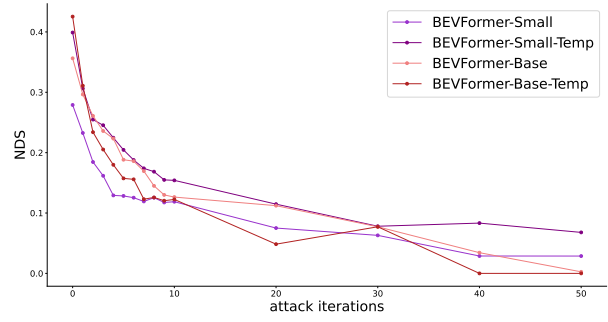
Table 6. Universal patch black box attacks: full results of mAP. X-axis represent target model and Y-axis represent source white box model.

Adversarial Source	BEVFormer	DETR3D	PETR	FCOS3D	PGD-Det	BEVDet	BEVDepth
Random Noise	0.3179	0.3746	0.2857	0.2776	0.2919	0.2670	0.3206
BEVFormer	0.3141	0.3589	0.2648	0.2475	0.2696	0.2254	0.2965
DETR3D	0.3235	0.3609	0.2566	0.2264	0.2592	0.2177	0.2876
PETR	0.2954	0.3412	0.1890	0.2127	0.2396	0.1769	0.2804
FCOS3D	0.2604	0.3149	0.1125	0.1473	0.1669	0.1461	0.2336
PGD-Det	0.2811	0.3350	0.2315	0.1733	0.1670	0.1552	0.2080
BEVDet	0.3079	0.3672	0.2715	0.2734	0.2807	0.2551	0.3131
BEVDepth	0.3140	0.3655	0.2687	0.2648	0.2750	0.2467	0.3011

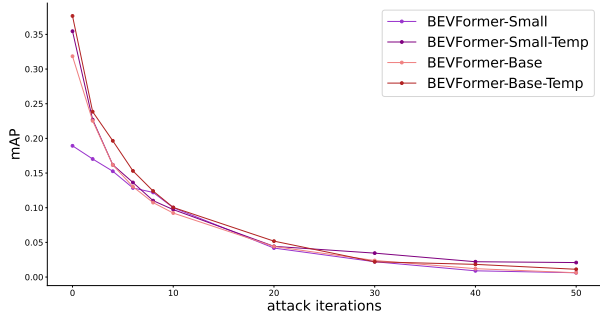
Table 7. Universal patch black box attacks: full results of NDS. X-axis represent target model and Y-axis represent source white box model.



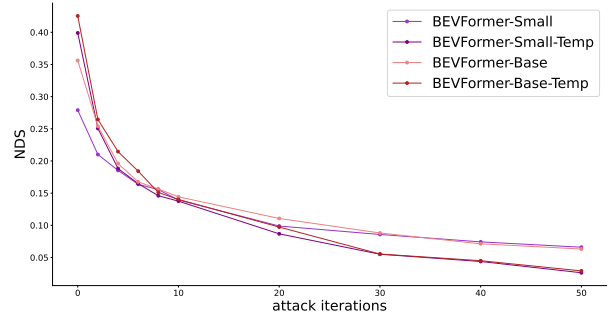
(a) Pixel-based untargeted attacks: mAP vs. attack iterations



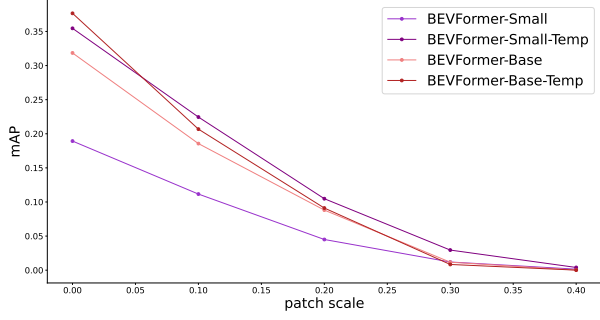
(b) Pixel-based untargeted attacks: NDS vs. attack iterations



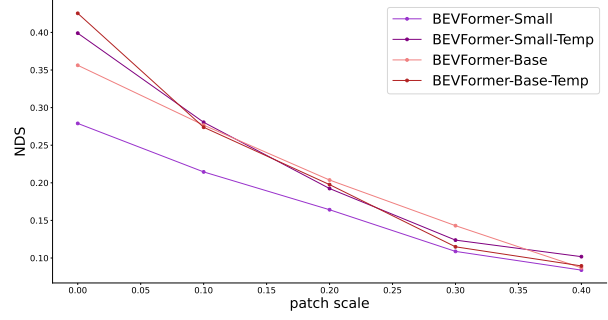
(c) Pixel-based localization attacks: mAP vs. attack iterations



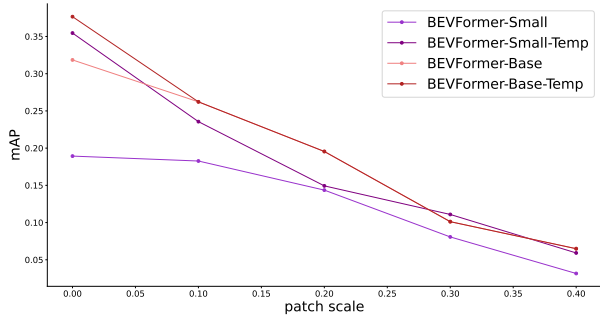
(d) Pixel-based localization attacks: NDS vs. attack iterations



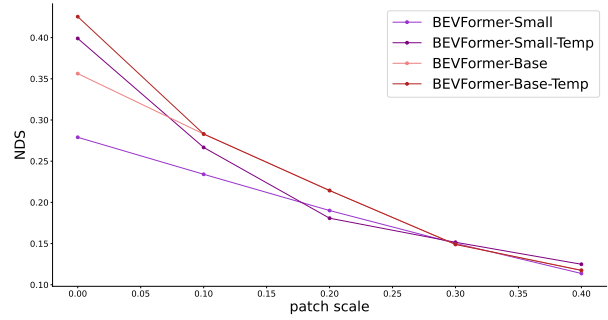
(e) Patch-based untargeted attacks: mAP vs. patch scale



(f) Patch-based untargeted attacks: NDS vs. patch scale

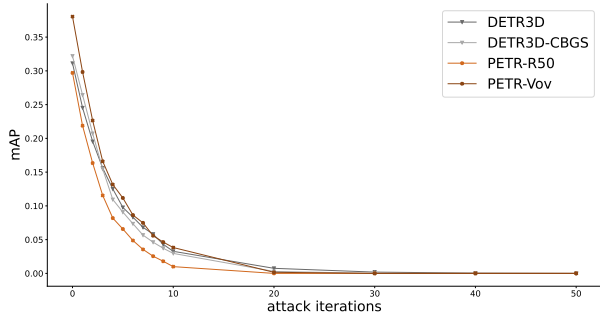


(g) Patch-based localization attacks: mAP vs. patch scale

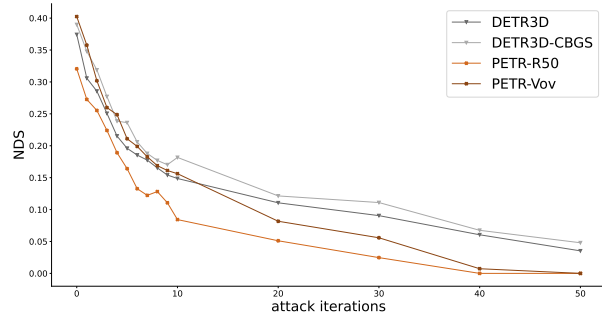


(h) Patch-based localization attacks: NDS vs. patch scale

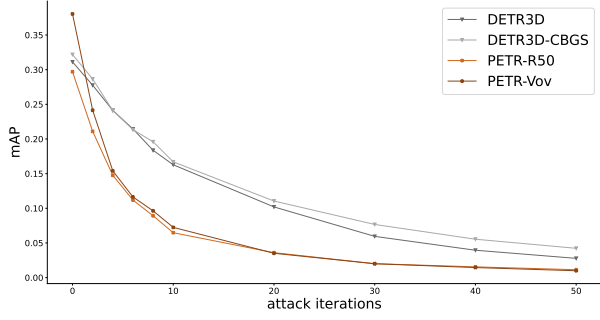
Figure 9. BEVFormer full results



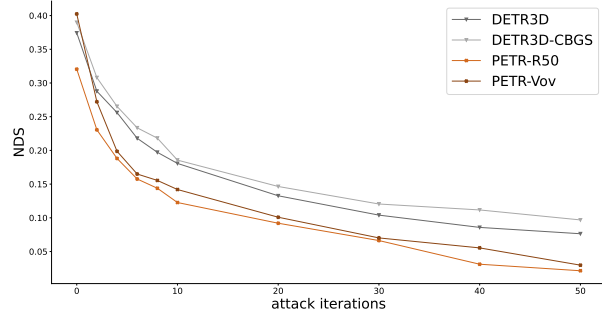
(a) Pixel-based untargeted attacks: mAP vs. attack iterations



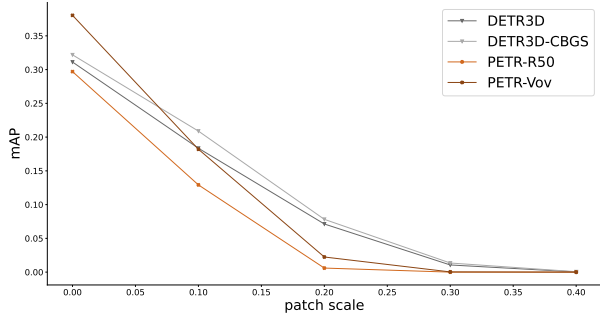
(b) Pixel-based untargeted attacks: NDS vs. attack iterations



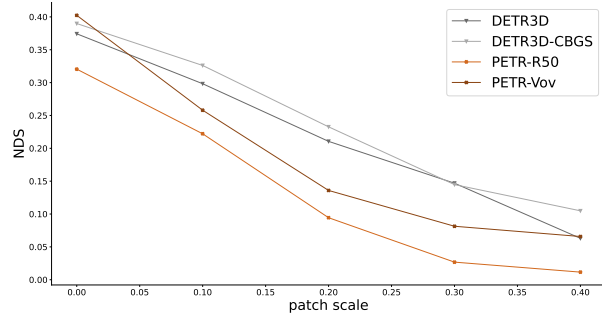
(c) Pixel-based localization attacks: mAP vs. attack iterations



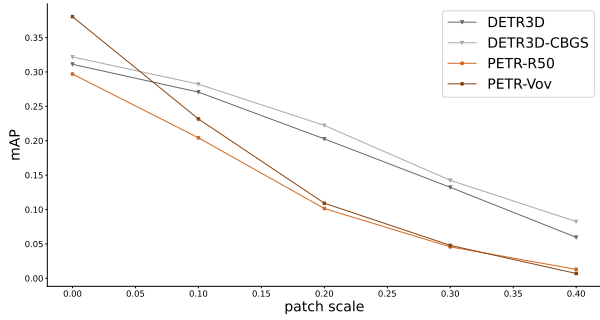
(d) Pixel-based localization attacks: NDS vs. attack iterations



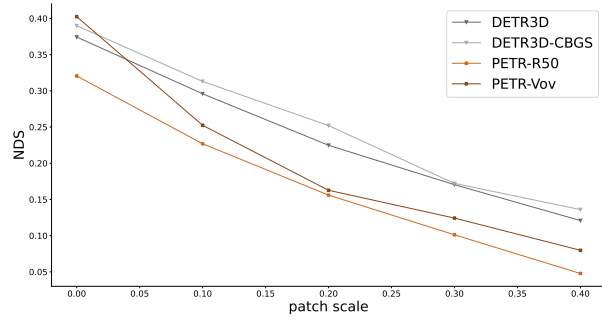
(e) Patch-based untargeted attacks: mAP vs. patch scale



(f) Patch-based untargeted attacks: NDS vs. patch scale

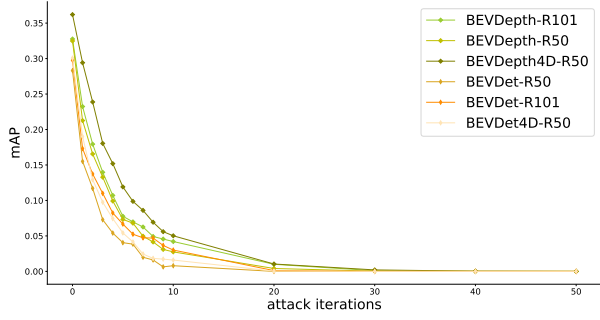


(g) Patch-based localization attacks: mAP vs. patch scale

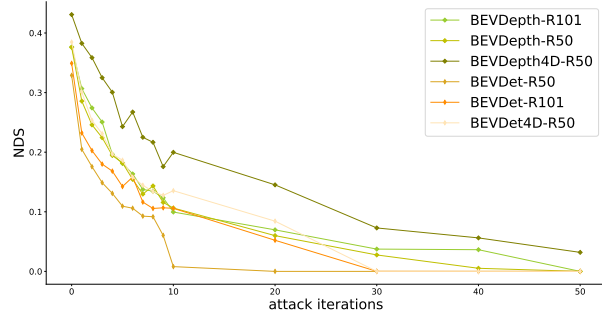


(h) Patch-based localization attacks: NDS vs. patch scale

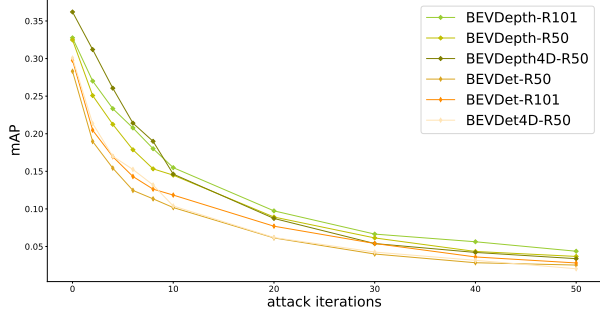
Figure 10. DETR3D and PETR full results



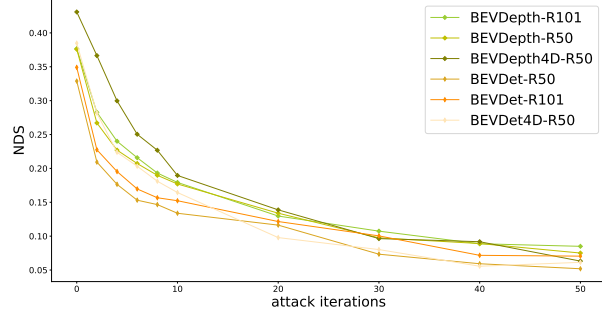
(a) Pixel-based untargeted attacks: mAP vs. attack iterations



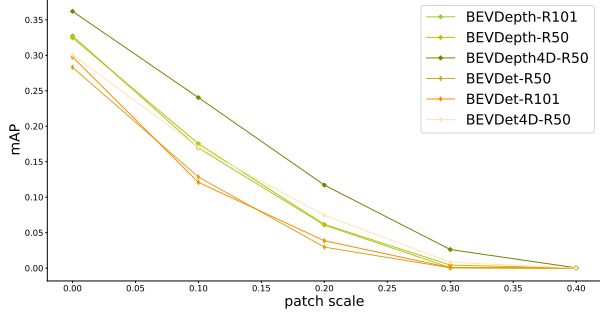
(b) Pixel-based untargeted attacks: NDS vs. attack iterations



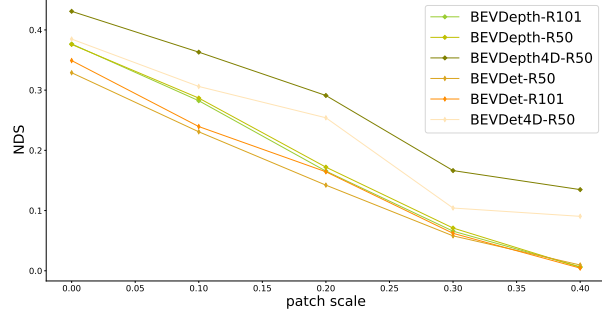
(c) Pixel-based localization attacks: mAP vs. attack iterations



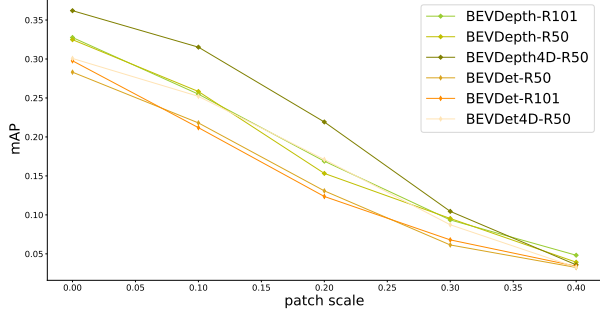
(d) Pixel-based localization attacks: NDS vs. attack iterations



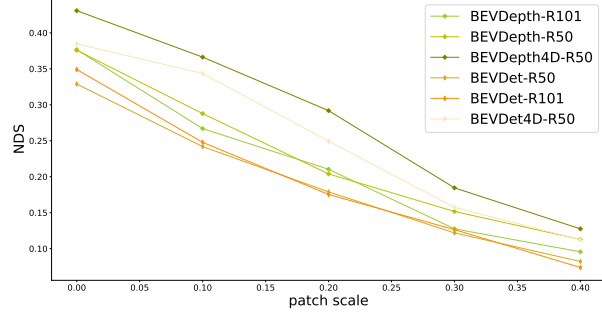
(e) Patch-based untargeted attacks: mAP vs. patch scale



(f) Patch-based untargeted attacks: NDS vs. patch scale

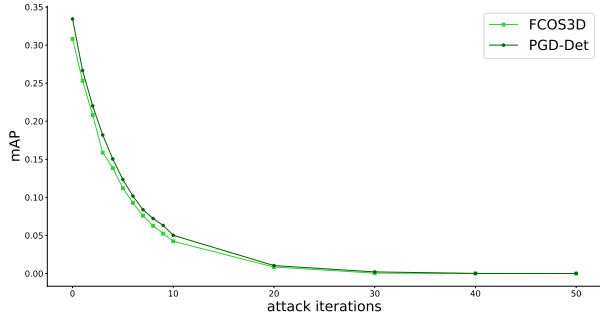


(g) Patch-based localization attacks: mAP vs. patch scale

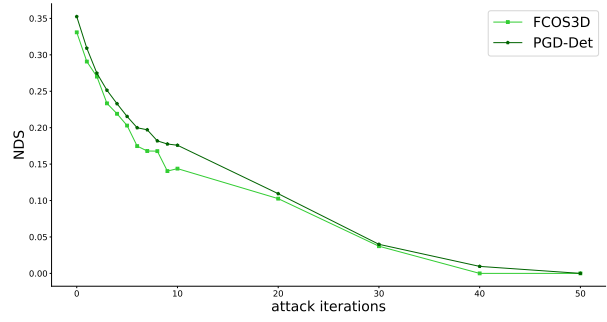


(h) Patch-based localization attacks: NDS vs. patch scale

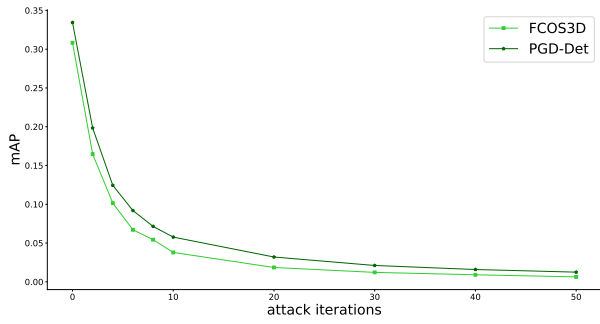
Figure 11. BEVDet and BEVDepth full results



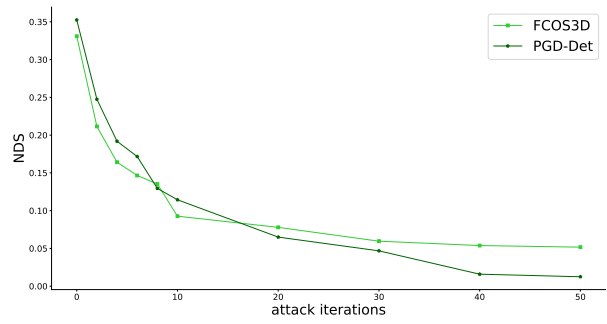
(a) Pixel-based untargeted attacks: mAP vs. attack iterations



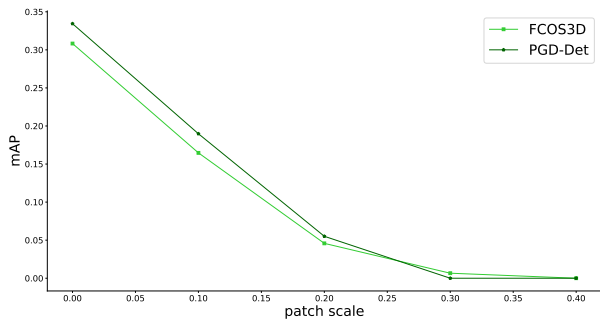
(b) Pixel-based untargeted attacks: NDS vs. attack iterations



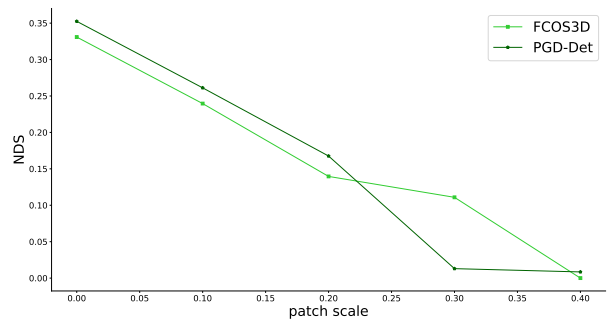
(c) Pixel-based localization attacks: mAP vs. attack iterations



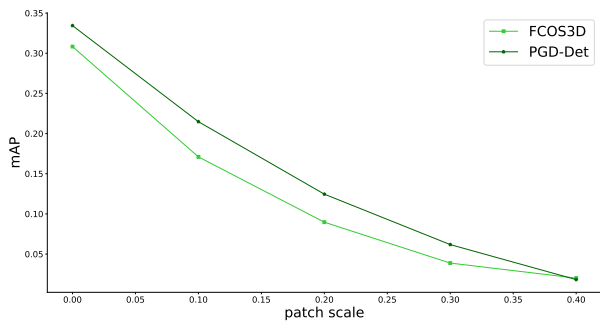
(d) Pixel-based localization attacks: NDS vs. attack iterations



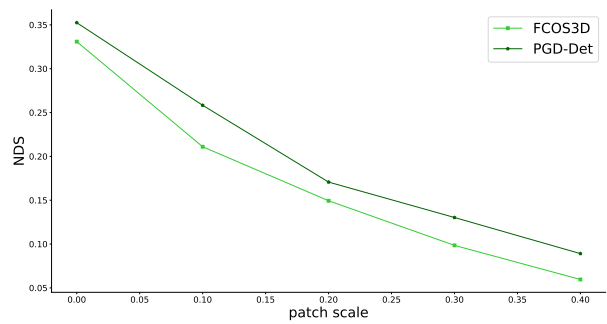
(e) Patch-based untargeted attacks: mAP vs. patch scale



(f) Patch-based untargeted attacks: NDS vs. patch scale



(g) Patch-based localization attacks: mAP vs. patch scale



(h) Patch-based localization attacks: NDS vs. patch scale

Figure 12. FCOS3D and PGD full results